Co-published by
Institute of Fluid-Flow Machinery
Polish Academy of Sciences
Committee on Thermodynamics and Combustion
Polish Academy of Sciences

http://www.imp.gda.pl/archives-of-thermodynamics/

Liquid crystal thermography supported by PIV and DII as modern and unique tools for technical and biomedical research and diagnosis – mini review

Jan A. Stąsiek, Michał E. Klugmann*, Dariusz P. Mikielewicz

Gdańsk University of Technology, Faculty of Mechanical Engineering and Ship Technology, ul. Narutowicza 11/12, 80-233 Gdańsk, Poland
*Corresponding author email: michal.klugmann@pg.edu.pl

Received: 08.11.2024; revised: 19.01.2025; accepted: 24.01.2025

Abstract

Liquid Crystals Thermography, Particle Image Velocimetry, Infrared Imaging Thermography and Digital Infrared Imaging have been successfully used in non-intrusive technical, industrial and biomedical studies and applications. These four tools (based on the desktop computers) have come together during the past two decades to produce a powerful advanced experimental technique as a judgment of quality of information that cannot be obtained from any other imaging procedure. A brief summary of the history of this technique is reviewed, principal methods and tools are described and some examples are presented mostly from our own research. Automated data evaluation allows us to determine the heat and flow visualization and locate the area of suspicious tissue in the human body. Anyway with this objective, a relatively new experimental technique has been developed and applied to the study of heat and mass transfer and for biomedical diagnosis.

Keywords: Heat and mass transfer; Biomedical diagnosis; Liquid crystal; Laser anemometry; Infrared photography; Digital image processing

Vol. 46(2025), No. 1, 7–24; doi: 10.24425/ather.2025.154188

Cite this manuscript as: Stąsiek, J.A., Klugmann, M.E., & Mikielewicz, D.P. (2025). Liquid crystal thermography supported by PIV and DII as modern and unique tools for technical and biomedical research and diagnosis – mini review. *Archives of Thermodynamics*, 46(1), 7–24.

1. Introduction

The beginning of the 21st century is a time of intensive scientific and research work related to micro- and nanotechnology, highly efficient energy conversion technology and methods of limiting its impact on the degradation of the natural environment. Research teams dealing with heat and mass exchange must face new challenges in the design and construction of modern and highly efficient process devices even for biomedical screened. Typical and idealized cases given in the specialist literature are no longer sufficient to solve current technical or technological problems. To cite two of them as an example: cooling of gas turbine blades or cooling of electronic systems, associated with complex geometry, non-uniform boundary conditions, and the action of aggressive and usually non-stationary flow. To investigate temperature and then heat transfer coefficient distributions (usual in Nusselt number form) on film heated models in channels with ribs turbulators has already been conducted by Baughn et al. [1], Bergles [2], Ciofalo et al. [3], Fiebig [4], Fiebig et al. [5], Hippensteele et al. [6], Jacobi et al. [7], Jones et al. [8,9], Leiner et al. [10], Mikielewicz et al. [11], Simonich and Moffat [12], Stasiek et al. [13–17], Tanda et al. [18–21] and the ones investigated in [22–25]. Designers of thermal devices expect more precise information on local values of the heat transfer coefficient, not only its average values. The flow pattern produced by transverse vortex generators (ribs) was visualized using a planar beam of double-impulse laser tailored by a cylindrical lens and oil particles. Sequential images of the particles in

Nomenclature

B – blue as the basic spectral colour
G – green as the basic spectral colour
I – intensity of any colour
R – red as the basic spectral colour
H – hue
l – linear dimension
S – saturation
x – distance

Abbreviations and Acronyms

CCD – charge-coupled device
CCIR– Comité Consultatif International des Radiocommunications
CFRP– carbon fibre-reinforced polymer
ChLC– cholesteric liquid crystals
CMOS– complementary metal-oxide-semiconductor
CR – computer radiography
DII – digital infrared imaging
FPS – frames per second
HSI – hue, saturation, intensity (model)
IR – infrared radiation
LCT – liquid crystal thermography
MRI – magnetic resonance imaging
NDT – non-destructive testing
PIV – particle image velocimetry
RGB – red, green, and blue (colour model)
SLC – smectic liquid crystal
TLC – thermochromic liquid crystal

a cross-sectional plane taken with a charge-coupled device (CCD) video camera from the downstream side of the flow were stored on a personal computer to obtain distributions of velocity vectors by means of the particle image velocimetry (PIV) method developed by Hiller and Kowalewski [26], Kowalewski et al. [27−29], Raffel et al. [30], Tanaka [31] and Tropea et al. [32]. Also in experimental investigations of the film cooling effectiveness for model turbine blades, the liquid crystal thermography (LCT) technique is presented. The film cooling and visualization of the few different jets holes configurations in steady-state and transient performance were performed experimentally above all by Satta and Tanda [33], Borda et al. [34] and Ekkad and Singh [35]. Therefore with this objective, a new experimental technique has been developed and applied to the study of heat and mass transfer and also for biomedical diagnosis by application of colour images for skin examination. Automated evaluation allows us to determine the heat and flow visualization and locate the area of suspicious tissue in the human body [36]. In medical case, the use of digital infrared imaging (DII) and LCT is based on the principle that metabolic activity and vascular circulation in both pre-cancerous tissue and the area surrounding a developing breast cancer is almost always higher than in normal breast tissue. These temperature variations may be among the earliest signs of breast cancer or orthopaedic cases and/or a pre-cancerous state of the breast as presented in [37−42] and the recently presented study by Kesztyüs et al [43]. These expectations are met by automated and fully computerized LCT based on the physicochemical properties of, among others, helical cholesterol esters, digital-computer and analogue analysis of colour images. It enables not only the study of complex geometries or the influence of non-uniform boundary conditions, but also pulsating and turbulent flows of large scales and low frequencies. Situations of such complex heat exchange can be found in most devices in which energy conversion processes take place. The analog-digital liquid crystal thermography supported by PIV [32] are excellent and recognized measurement methods used to study advanced thermal and flow processes in major scientific centres in the world and in Poland. LCT theoretically enables visualization of two-dimensional temperature and velocity fields with single-pixel accuracy and learning about the influence of many thermophysical and flow factors on the formation of laminar and turbulent boundary layers [44−53]. Organisation of scientific research using liquid crystal thermography and image anemometry will allow verification of established stereotypes in measurement techniques and empirical relationships obtained on the basis of low-precision (global) measurements, but still used in engineering practice and medical research [37,38].

2. RGB and HSI colour models

The perception of the spectrum of electromagnetic waves (colours) is an individual phenomenon. The colour of the setting sun at the same time can be interpreted by different people as red, dark red or light red. The variety of colour definitions indicates the different sensitivity of the human eye to absorbing light, photosensitive retinal receptors and colour perception. The problem of unambiguous colour description complicates the way and methods of defining colours, as in everyday Polish hue and colour are synonyms.

Colour is perceived thanks to photosensitive cells in the retina of the eye, called rods and cones. Rods are sensitive to the degree of quality (scotopic vision), and cones to colour (photopic vision). The human eye has its limited colour resolution, i.e. sometimes it is unable to see the difference between two colours with different spectrums, treating them as the same. It shows a different degree of sensitivity to a specific colour, which is determined by the individual and knowledge in using the sense of sight. The human eye contains three types of cones, with different spectral characteristics. Three dyes participate in the perception of colours, reacting with different sensitivities to the wavelength of electromagnetic radiation [54]:

- erythrolabe – sensitive mainly to the wavelength corresponding to red,
- chlorolabe – sensitive mainly to the wavelength corresponding to green,
- cyanolabe – sensitive mainly to the wavelength corresponding to blue.

On this basis, the RGB colour model was developed, widely used in devices analysing and displaying images, such as digital cameras, camcorders, monitors and televisions, etc. It is obvious to manufacturers and users of colour monitors, cameras and computer graphics that colour is a combination of three basic colours (primary colours) – red, green and blue (RGB). Additive

mixing of primary colours, i.e. RGBs, allows obtaining "millions" of colours of visible light. The history of research and considerations on the essence of colours and their impact on humans is much longer than the history of research on the properties of electromagnetic radiation.

Considerations on the creation of colours and their qualifications were undertaken by, among others, Pythagoras, Aristotle, Plato, Robert Grosseteste, Leon Battista Alberti and Leonardo da Vinci. A breakthrough in the study of colour was the discovery of Isaac Newton, made during his research on the dispersion of white light in a prism and the reverse process, during which he obtained white light again [54]. The colour triangle, drawn up in the mid-19th century by James Clerk Maxwell (1831–1879), illustrating the method of obtaining different colours by an appropriate combination of three primary colours: red, green and blue placed at the vertex of the triangle, became the basis for the technology of colour printing, photography and colour television. The colour system proposed by Maxwell and the scientific considerations conducted by his successors led to the establishment of a standardized colourimetric system in 1931 by the International Commission on Illumination (Commission Internationale de l'Eclairage – CIE) [55]. The CIE 1931 system and its later version CIE 1976 (Fig. 1), derived from Maxwell's triangle, are based on the recognition of red (*R*), green (*G*) and blue (*B*) as the basic spectral colours, which are described in the standardized trichromatic coordinate system *X*, *Y*, *Z*, also known as relative visual efficiency of cones. Due to the individual (individual) perception of colours by humans, many digital models describing the space of colours visible to humans have been developed. One of the more successful and used models is HSI (hue, saturation, intensity):

- hue (*H*) – specifies numerical shades of colour (on an angular scale from 0 to 360°),
- saturation (*S*) – is the saturation, deviation of the colour from white,
- intensity (*I*) – is the quality of colour, which indicates whether the colour is closer to white or black.

This model assumes that colours perceived by humans can be described using these three coordinates, provided that the points are located on the surface of a solid of a double-sided cone.

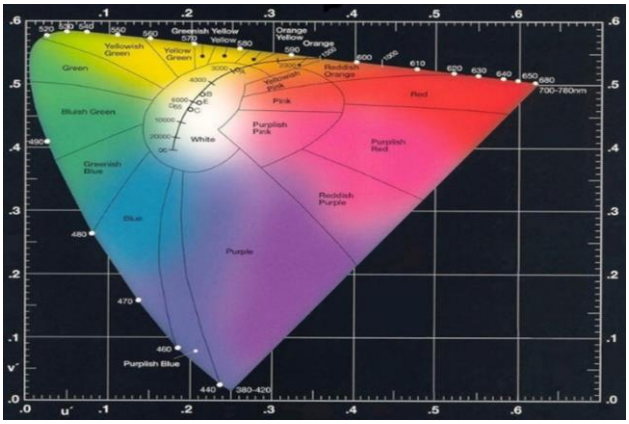

Fig. 1. The map of the 1976 chromaticity diagram is similar in nature to the triangle colour map. At the end points of the chart, the colour primaries (as defined by the CIE in 1976) are shown [55].

Figures 2 and 3 show two models of colour description: the first is based on the traditional model built on a cube, in which the basic colours are assigned to the appropriate corners of the solid, and the second is based on the HSI (Hue, Saturation and Intensity) model, where the intensity axis changing from black to white is marked and a cross-section of the solid is shown corresponding to the changing values of colour (*H*) and its saturation (*S*).

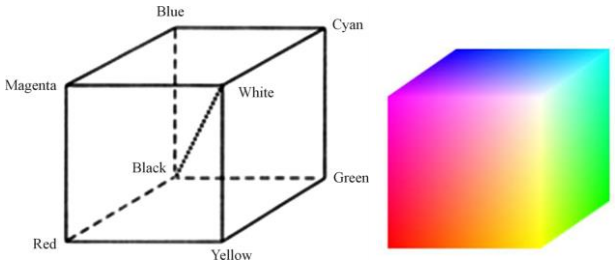

Fig. 2. RGB colour model.

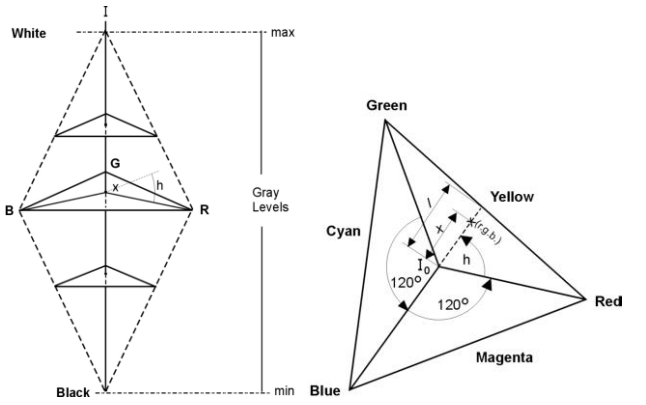

Fig. 3. HSI colour model.

Mathematically, it is relatively simple to change the colours of the image from the RGB model to the HSI model. If the coordinates of the colours or "hues" are defined by the coordinates as in Fig. 3, the intensity of any colour is defined by the formula:

$$I = \frac{R+G+B}{3}. \quad (1)$$

Accordingly, hue (colour) is represented by the angle of the vector rotating about the white colour point located inside the CIE 1976 colour map from the origin, which defines the colour red (Fig. 3 down). This value is given by the formula:

$$H = \frac{1}{360}\left[90 - \arctan\left(\frac{F}{\sqrt{3}}\right) + \{0, G > B; 180, G < B\}\right], \quad (2)$$

where:

$$F = \frac{2R-G-B}{G-B}. \quad (3)$$

The colour saturation is appropriately determined by the formula (4) in the following form:

$$S = 1 - \left[\frac{min(R,G,B)}{I}\right] = \frac{x}{l}. \quad (4)$$

For example, in Eq. (4), assuming the smallest values of R/I, G/I and B/I equal to 1, we get a saturation of 0, which means white. When using an 8-bit computer, all the values or attributes of colours change from 0 to 255. Colour image processing can be much less complicated and quicker to execute if colour images captured from RGB video sources can be digitally converted from RGB data to HSI data reported in [54,56,57].

The saturation of a chosen hue can be decreased by moving away from the pure hues parameter of the diagram toward its centre to the point where red, green and blue mix equally into white. Each step toward the diagram's centre represents a decrease in saturation [55].

3. Thermochromic liquid crystal

The history of research on liquid crystals dates back 120 years. In 1888, Austrian botanist F. Reinitzer [36] accidentally discovered the "anomalous" behaviour of cholesterol benzoate when heated. This compound melted at 145.5°C. However, the resulting liquid was not clear, had a very high viscosity and showed colour effects. Only at 177.5°C did it transition to a transparent liquid. German physicist O. Lehmann [58] became interested in this phenomenon, considering the state of the turbid liquid to be a separate state of matter, to which he gave the name liquid crystal. Currently, an alternative term is also in use – mesophase (from the Greek mezos – intermediate). The liquid crystal phase is characterized by rheological properties similar to those of liquids (the lack of a rigid crystal lattice causes a lack of elasticity of shape and allows flow), although it usually has significant viscosity. At the same time, however, liquid crystals exhibit anisotropy of physical properties, which means that physical quantities measured in different directions take different values. This feature is characteristic of solid crystals and does not occur in liquids, with the numerical anisotropy values generally being lower for liquid crystals than for solids. For many years, liquid crystals were treated as a kind of physical curiosity, and it was not until the 1960s that research on these substances began to develop rapidly, related to their role in biological systems and technical applications. Most applications of liquid crystals are based on the ease with which relatively weak external stimuli can change the macroscopic properties of the liquid crystal. This allows for the construction of devices that detect changes in various physical quantities and electronically controlled information imaging systems. Cholesteric liquid crystals (ChLC), after several decades of collecting research material, found application in science and technology, initially in thermography and defectoscopy, and then in the detection of organic compound vapours, electromagnetic radiation and ultrasound.

3.1. Structure and classification

At present, many different structures occurring in liquid crystal states are known. Due to the method of obtaining, liquid crystals are divided into thermotropic - formed after melting solid crystals and lyotropic – formed after dissolving a mesogenic substance in a suitable solvent. The thermotropic mesophase can be enantiotropic – occurring during heating and cooling or monotropic – if it appears only during cooling of the substance from the isotropic liquid state [54].

The order of molecules in the liquid crystal state depends on their shape, molecular properties and the nature of intermolecular interactions. The vast majority of molecules of mesogenic compounds have the shape of elongated rods or flat disks. Substances with elongated molecules can form a smectic mesophase, i.e. a smectic liquid crystal (SLC). In this type of mesophase, the molecules lie in mono- or bimolecular layers equally spaced from each other. Within one layer, there may also be various types of constraints imposed on the mutual position of the centres of gravity of the molecules, which distinguishes different types of smectic phases. The unit vector n parallel to the local average direction of the order of the long molecular axes – the so-called director, is in smectic either approximately perpendicular to the planes of the smectic layers or inclined to them at a certain angle. Individual types of smectic phases are usually described by capital letters of the Latin alphabet.

Elongated molecules can also form nematic order, i.e. nematic liquid crystal (NLC). In this type of liquid crystal phase, the molecules are free to rotate around the long molecular axis and translate, maintaining approximately the order relative to neighbouring molecules (Fig. 4).

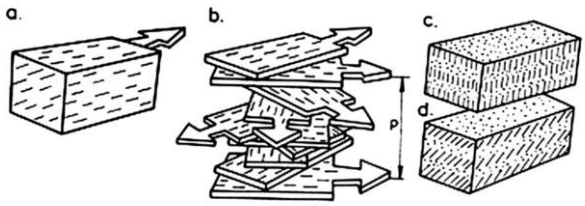

Fig. 4. Molecular arrangement in different types of mesophases. The direction n is represented by arrows: a) nematic, b) cholesteric, c) smectic A, d) smectic C.

If the molecules of a mesogenic compound have a centre of structural asymmetry (they are chiral), then due to the presence of spatial obstacles, the substance takes on a molecular order that is not nematic but twisted nematic, also called cholesteric. In a twisted nematic, the molecules lie in monomolecular layers, within which the order is quasi-nematic, as a result of which the molecular structure takes the shape of a screw (helicoids) as shown in Figure 4b. Such a twisted structure is equivalent to a nematic, but it determines the existence of several specific physical properties. The name ChLC is increasingly replaced by the one given above – twisted nematic.

3.2. Applications of ChLC

For the practical application of cholesteric liquid crystals (ChLC), optical phenomena that are characterized by significant sensitivity in response to external stimuli are of primary importance. Selective reflection of light and optical activity and circular dichroism should be mentioned here. The most frequently measured quantities are: temperature of occurrence of colours or colour transitions, wavelength of maximum selective reflection, intensity of selectively reflected light. The selection of the measurement method is determined by substantive and functional needs (including the required accuracy and sensitivity

of the measurement, time, costs and conditions of its performance and method of recording results). B&H Liquid Crystal Devices Ltd [59] presents some applications of ChLC depending on the working temperature.

In medicine, thermography was used, for example, when taking thermograms of the eye and eye socket. Using a solid layer of ChLC applied or by applying a thermographic foil, it is possible to determine the boundaries of the inflammatory process and detect separate foci of inflammatory infiltrates at different stages of their development. In comprehensive examinations of patients, liquid crystal thermography allows for obtaining information about the location of purulent-inflammatory foci, malignant and non-malignant tumours, as well as their metastases to lymph nodes and lymphatic vessels. This method enables observation of changes in the inflammatory state and allows the selection of the most rational surgical access to the inflammatory focus. Cancerous tissue emits significantly more energy than normal tissue. Rapid cell division is associated, among other things, with increased metabolism, which causes an increase in temperature and can be detected visually using thermography. In the case of breast cancer in women, a temperature increase of 0.5 K is often a sign of a benign tumour, while an increase of 2 K suggests a malignant tumour. In material testing, non-destructive testing (defectoscopy) with methods such as X-ray, ultrasound or magnetic resonance occupy an important place. In recent years, there has been development of device defectoscopy based on the use of liquid crystal thermography.

The distribution of temperature measured on the surface of an object is related to the properties of the material and the operating characteristics of the device. The temperature distribution is influenced by both the amount of heat dispersion (thermal dissipation) and thermal diffusivity. A typical example of the use of this method is the location of damage in joints. There is a high current density at the fault site, and therefore a high temperature, so it can be located very precisely.

3.3. Calibration of ChLC

Before starting temperature measurements and data recording with a computer-vision system, the characteristics of the measuring section consisting of a liquid crystal layer, light sources and a camera-video-computer system must be determined. It should be done on an experimental stand so that the optical conditions during calibrations and then the experiment are comparable. Both the temperature range of the colour response and the colour response temperature can be selected depending on the needs of the experiment in the range from –30°C to +120°C with a temperature range from 0.5°C to 20°C.

The type of liquid crystal selected for the experiment also depends on the type of means used to analyse the resulting colour images. In the described experiment, a computer-vision analysis technique is used that excludes the possibility of different interpretations of the same image depending on the way of perceiving colours. In such a case, the best material is a liquid crystal with a narrow temperature range. In the presented measurements, the liquid crystal film was manufactured by MERC Ltd. [57] The symbol R30C5WA means a colour response temperature range of 5°C and a colour response temperature of 30°C, i.e. the possibility of measurement in the temperature range from 30 to 35°C. The experimental stand for calibration of liquid crystal film is shown in Fig. 5. The layer of liquid crystal film is placed between a brass marking plate and an 8 mm thick plexiglass plate. This allows the change in the colour of the liquid crystal layer to be viewed through the plexiglass under the influence of changes in the temperature of the brass plate. The whole is insulated with a layer of polystyrene. The brass plate has dimensions of 210 × 170 × 8 mm. To obtain a linear temperature distribution in the characteristic plate, one end of it is cooled with thermostated water and the other is heated with an electric heater with adjustable power.

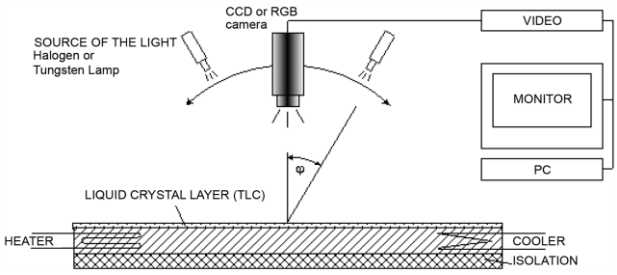

Fig. 5. Calibration brass plate with liquid crystal layer attached.

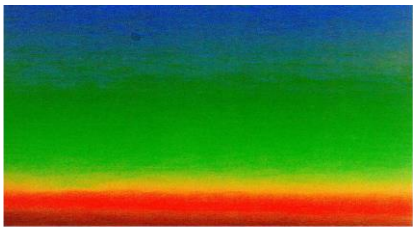

Fig. 6. The distribution of the colour component pattern on the liquid crystal layer measured by RGB colour camera.

For the applied R30C5WA liquid crystal layer as a foil with the colour component pattern (see Fig. 6), calibration was performed using halogen and tungsten lighting (Figs. 7 and 8). Analysis of the averaged values of the gauge curves showed that halogen lighting is more advantageous and useful for thermographic applications and it was selected for further measurement procedures.

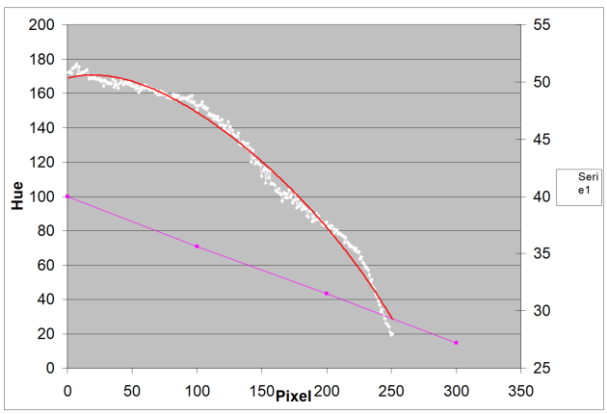

Fig. 7. Averaged value of the feature curves of the liquid crystal film under halogen illumination.

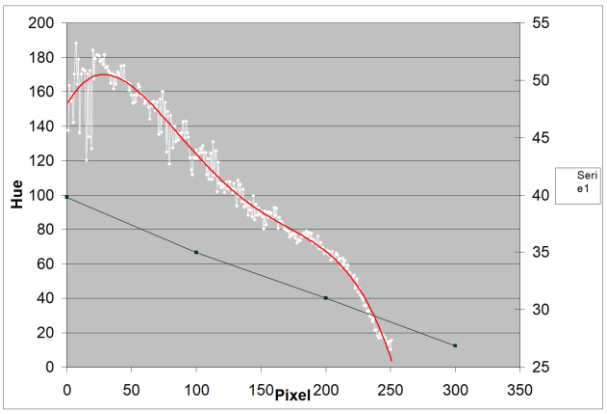

Fig. 8. Averaged value of the feature curves of the liquid crystal film under tungsten illumination.

3.4. Visualization of velocity and temperature fields in cavity

The liquid crystal technique is used not only in air flows, but also in other fluids. The distributions of the temperature field and velocity vectors were visualized using a liquid crystal in a pure solution form or microcapsules, both as trace particles inside the fluid or as a coating of the flowing surface. The encapsulated form of liquid crystal can be mixed directly with water, glycerine or silicone oil. It is recommended to create dilute solutions, i.e. 0.01–0.02% by weight [16,17]. Too much liquid crystal causes a milky colouration of the dilutes and when reflecting light, it causes blurring of colours. The structure of the flow together with the movement of the particles can be recorded using a photo camera or a video camera. With the flash of a white light knife "cutting through the flow" (similar to the PIV method), both the temperature of the coloured molecule and its flow direction (when several images of the same molecule are taken) can be recorded.

3.5. Particle Image Velocimetry

Digital image anemometry (known as Particle Image Velocimetry – PIV), as a measurement method of fluid mechanics, originates from visualization techniques used for hundreds of years, most often allowing only a qualitative assessment of the structure of the tested flow [30]. Visualization methods consist in observing marker particles, called seed particles, found in a moving fluid (e.g. smoke in the air, small pieces of wood in a river or specially selected particles in laboratory measurements) and determining, based on the observed movement of these particles, the nature of the flow of interest to us. The observation can be made here directly using the researcher's "eye" or using equipment enabling image recording. It is important that the observed marker particles are appropriately selected for the analysed movement – so that the tested flow "carries" them along with it. Their density must be close to the density of the flowing substance and their size must be suitably small. This will eliminate the influence of gravity and inertial factors and allow us to assume that the observed movement of particles is identical to the movement of the fluid carrying them. Most often, various types of powders, liquid droplets, smoke and pollen are used as seed particles, depending on the type of flowing medium (gas, liquid) and the nature of the flow. PIV consists in recording moving marker particles with a digital camera and further numerical analysis of the obtained image sequences, as a result of which we obtain instantaneous, full velocity fields of the moving fluid.

A typical diagram of the measuring techniques used in the PIV technique is shown in Fig. 9.

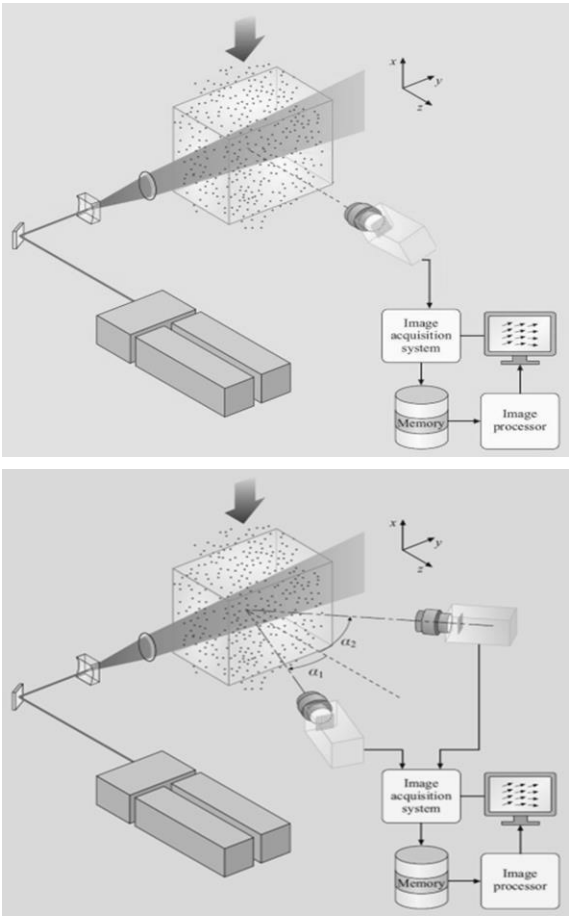

Fig. 9. Schematic of a typical PIV measurements with one camera (up), and two cameras (down) [32].

The tested flow with the addition of marker particles is illuminated by a narrow plane of light, the so-called light knife. Halogen lamps are used as the light source, and currently most often lasers, from which the light beam is directed at the tested flow by means of a system of mirrors and a cylindrical lens and formed into a light knife. The use of the light knife is intended to separate the tested, interesting cross-section of the flow from the rest of the measurement domain. Thanks to this, only the tested cross-section is visible on the recorded images, and the remaining part is darkened and not subject to recording. The obtained images of moving particles are subjected to further numerical analysis aimed at precisely determining their displacements between individual registrations. At present, the PIV measurements are performed by using small droplets of synthetic oil DEHS (Di-Ethyl-Heksyl-Sebacat). The oil drops volumetric concentration was very low hence they did not affect the flow structure.

The use of the PIV method entails certain limitations and conditions that must be met by images intended for analysis, namely:

- sufficiently high concentration of marker particles in images; a small number of particles does not allow the use of fast Fourier transforms (FFT),
- as even as possible saturation and brightness of the recorded images; large changes in the degree of exposure within the analysed area introduce the need to use filtering, which should average the brightness over the entire image,
- large differences in speed between individual image fragments favour the occurrence of interferences and distortions in the obtained velocity field, which occur when a larger number of lifted markers leave the analysed area due to too high speeds,
- the time interval between successive images should not be too small; small displacements have a directly proportional effect on measurement inaccuracies.

The path between obtaining digital images and obtaining vector graphs that are a graphical representation of velocity fields leads through a series of activities performed by a computer program; from manipulating graphic files, through typical mathematical operations, to using the functions controlling the system's graphical interface to visualize vector graphs. Mathematical calculations mainly come down to determine the correlation coefficients of image fragments in order to find particle displacements, and to convert them into velocity fields. In digital image anemometry, FFT is used to determine image correlation. These are algorithms for numerical calculation of the Fourier transform and the inverse Fourier transform.

4. IR Photography (IRP)

Infrared radiation as presented in Fig. 10 [60] can be used to remotely determine the temperature of objects and for imaging using differences in the thermal radiation of bodies [32]. For bodies at room temperature, this technique is called thermography, and for hot bodies, pyrometry. Thermography is used primarily in military and industrial applications, but the technology is reaching the public market in the form of infrared cameras. The most popular and comprehensive thermal cameras available for industrial and commercial buildings or energy conversion devices are FLIR products.

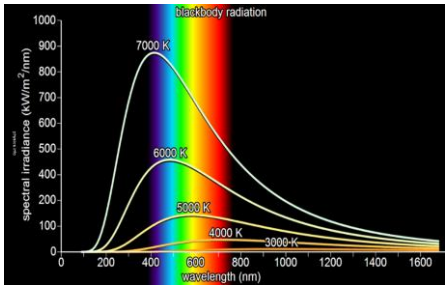

Fig. 10. Spectral irradiance graphs as a function of wavelength and temperature.

The FLIR T440bx thermal camera is based on infrared radiation and used in current investigations (Fig. 11). It offers all the latest FLIR features in a brilliant resolution. The real standout for the T440bx camera is FLIR's new MSX Thermal Image Enhancement. Multispectral imaging camera (MSX) combines the thermal and visible images into one data-rich image a completely new fusion technology. Easily identify intersecting walls, mechanical data plates and heat transfer elements or even whole furnaces and combustion systems, all while still viewing in full infrared. The FLIR T440bx series also offers a flexible, efficient and variably universal method of gathering and analysing equipment data with its high temperature range (–20°C to 650°C), multiple hot spot measurements, humidity and dew point measurements, wi-fi connectivity and sensitive to 0.03°C temperature changes.

Fig. 11. FLIR's T440bx IR camera.

In general, taking into account the advantages and disadvantages of this measurement technique, objects emit infrared radiation across a spectrum of wavelengths, but sometimes only a limited region of the spectrum is of interest because sensors usually collect radiation only within a specific bandwidth. Thermal infrared radiation also has a maximum emission wavelength, which is inversely proportional to the absolute temperature of the object, in accordance with Wien's displacement law. Therefore, the infrared band is often subdivided into smaller sections.

5. Experimental open wind tunnel

The experimental open wind tunnel was designed and constructed at the Institute of Energy of the Gdańsk University of Technology [11]. Thanks to its universal design, it allows for testing a wide range of geometries with a small expenditure of resources needed to adapt the measurement section to subsequent experiments. Figure 12 shows a diagram of the wind tunnel for modelling of heat exchanger elements.

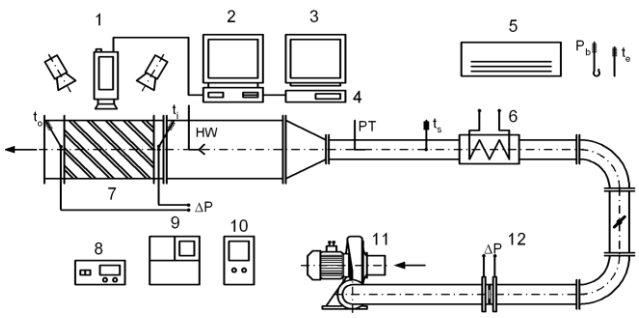

Fig. 12. Open low speed wind tunnel, 1 – RGB camera (TK-1070), 2 – PC, 3 – monitor (RGB-VMR 200), 4 – recorder/backup, 5 – air conditioning system, 6 – heater, 7 – LC mapping section, 8 – digital micro-manometer FC012, 9 – DISA hot wire system (HW), 10 – variac, 11 – fan, 12 – orifice, PT – Pitot tube.

In the air preparation section, an MPA 90T fan is installed with a maximum capacity of 1200 nm^3/h with automatic and smooth regulation of the rotational speed using an inverter, which allows for obtaining Reynolds numbers Re of up to approximately $1.5 \cdot 10^5$ in the measurement rectangular section (D_h = 69.11 mm).

The fan is connected by a steel spiral pipe to the heater and then to the control section. Thanks to the placement of the orifice with a dial measurement (D = 100 mm, d = 50.12 mm and module m = 0.2512), it is possible to estimate the amount of air flowing through the station before the heater, whose regulated power (N = 1800 W) allows heating the compressed air to the desired temperature.

The air prepared in this way is forced into the control section made of 8 mm thick plexiglass. Initially, it is a tube with a diameter of d = 90 mm and length of L_1 = 1080 mm, then a diffuser with a length of L_2 = 330 mm and a rectangular stabilizing section with a length of L_3 = 810 mm. Inside the round channel, a control measurement of the amount of air flowing and its parameters is carried out using a Pitot tube and a digital micromanometer FC012 from Furness Controls Limited UK. This part of the control section is also used to calibrate the wire anemometer probe (DISA-thermo-anemometer type 55M01), which is used to measure the height of air turbulence at the inlet to the measuring section during the experiment.

The modelling (mapping) section, is supplied via a bypass valve which allows the hot air supply to be cut off if necessary. The modelling section is illuminated from above by a set of tungsten or halogen lamps and the colour images are recorded by using a computer vision system.

The mapping section, which is an 8 mm thick plexiglass plate and a 0.15 mm thick liquid crystal foil, is washed by the air flowing around that supplies heat to the ribbed surface. Know-ledge of the heat flux density and local temperature values obtained using liquid crystal thermography enables the calculation of local values of heat transfer coefficients and then Nusselt numbers using the gauge curve of the liquid crystal layer (Fig. 7) [17–19].

Thermographic measurements of stationary and non-stationary two-dimensional temperature fields in the measuring section of the model heat exchanger were aimed at determining the heat transfer coefficients and the Nusselt number. Local surface temperatures were assessed based on hue measurements, which were then converted into the temperature in Kelvin or Celsius scale using the gauge curve of the liquid crystal layer. In many cases, as mentioned above, remarkable enhancement of local and spatially averaged surface heat transfer rates is possible with rib turbulators, in spite of the lower local Nusselt number at certain locations along the ribbed surfaces.

The test surface that is analysed contains a collection of rib turbulators that are perpendicular and angled with respect to the flow stream (Fig. 13) [13,14]. However, to determine the surface heat flux, the convective power is provided by the thermofoil heaters.

Spatially resolved temperature distributions along the bottom rib turbulator test surface are determined using a liquid crystals foil and true-colour image processing system commercially available from Data Translation Ltd. [56] and Hallcrest [54].

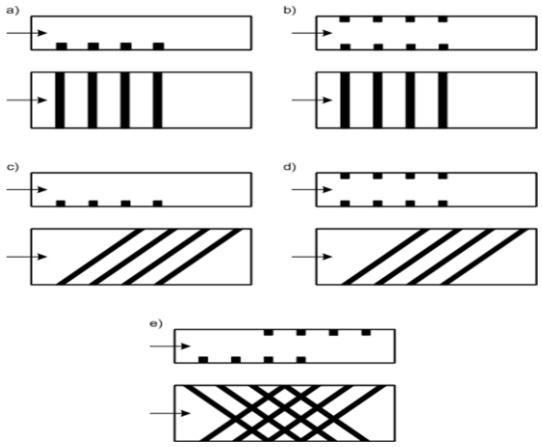

Fig. 13. Schematic view of four types of transverse vortex generators.

6. Examples of experimental results

In the following examples, the TLC's foil sheet and unsealed TLC's tracers have been applied to measure both the surface temperature and velocity, and temperature fields in a glycerol-filled cavity under free convection. For human body screening or biomedical situations, few images using Thin Layer Chromatography (TLC) and IR-Photography techniques are also presented.

6.1. Temperature measurement on the ribbed surface and square section column

Figures 14 and 15 show photographs of the colour distribution of the liquid crystal layer on the ribbed surface and around a square section column. A pattern of the Nusselt number Nu reconstructed by false colour images of the heat transfer from a surface with square columns is presented in Fig. 16.

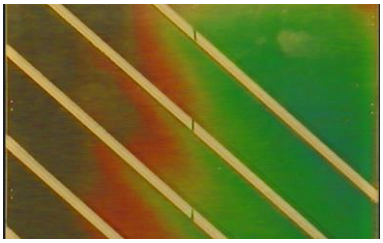

Fig. 14. Photograph of the colour distribution of the liquid crystal layer on the ribbed surface.

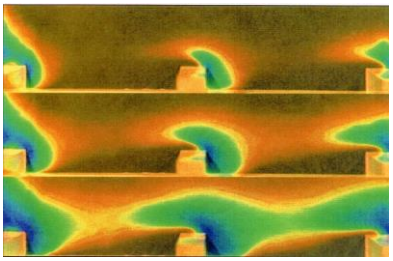

Fig. 15. Photograph of the colour distribution of the liquid crystal layer around a square section column.

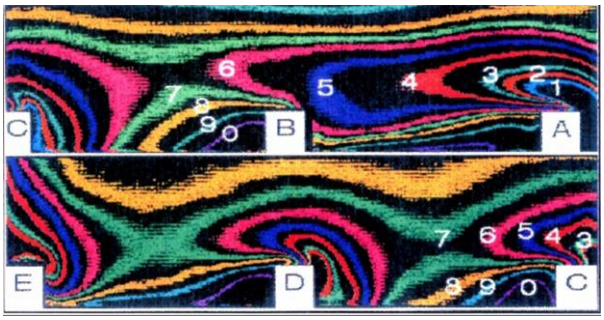

Fig. 16. Pattern of the Nusselt number Nu reconstructed by false colour images of the heat transfer from surface with columns for Re = 20 000 (No. 0: Nu = 79; 9: 99; 8: 113; 7: 123; 6: 136; 5: 147; 4: 160; 3: 175; 2: 185; 1: 209).

Figures 17 and 18 show (for geometry a and b, see Fig. 13) the local streamwise Nusselt number distribution between the selected ribs (out of several dozen) of the central zone of the model heat exchanger. Thermal flow tests were performed for four values of the Reynolds number, i.e. 9000, 16 000, 26 000 and 35 500. The analysis of the experimental results showed that flow turbulisation using simple transverse ribs leads to the best effects (the highest average values of the heat transfer coefficient are obtained for the perpendicular ribs). Turbulators set at angles other than perpendicular to the air flow contribute to the improvement of heat exchange to a lesser extent.

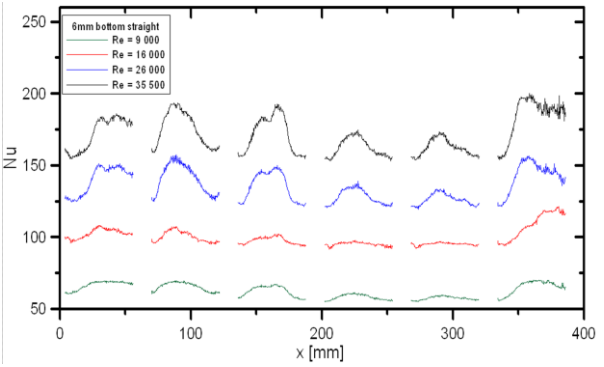

Fig. 17. Local streamwise Nusselt number distribution between the ribs in the boundary layer for ribbed bottom walls and ribs perpendicular to the flow (configuration a in Fig 13) [13].

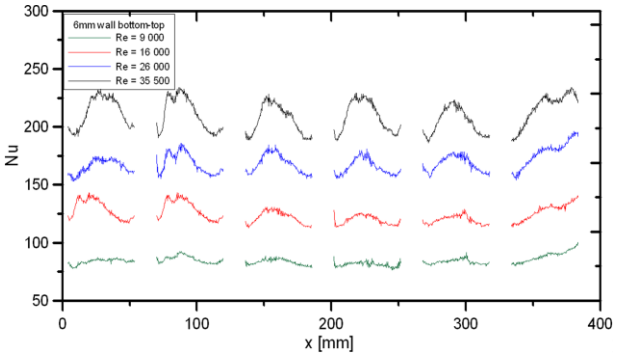

Fig. 18. Local streamwise Nusselt number distribution between the ribs in the boundary layer for ribbed bottom and top walls and ribs perpendicular to the flow (configuration b in Fig. 13) [13].

6.2. PIV measurements

For the numerical verification of local and averaged thermographic measurements of Nusselt numbers, knowledge of the turbulence level and flow velocity is required. These values can be obtained based on PIV anemometric measurements (Fig. 19). The sample results are presented in Fig. 20. The area scanned by the PIV method was in all cases located in the mid-vertical plane between side walls.

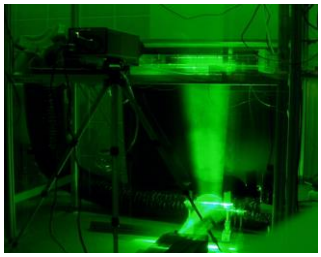

Fig. 19. Laser light sheet visualisation during a velocity measurement.

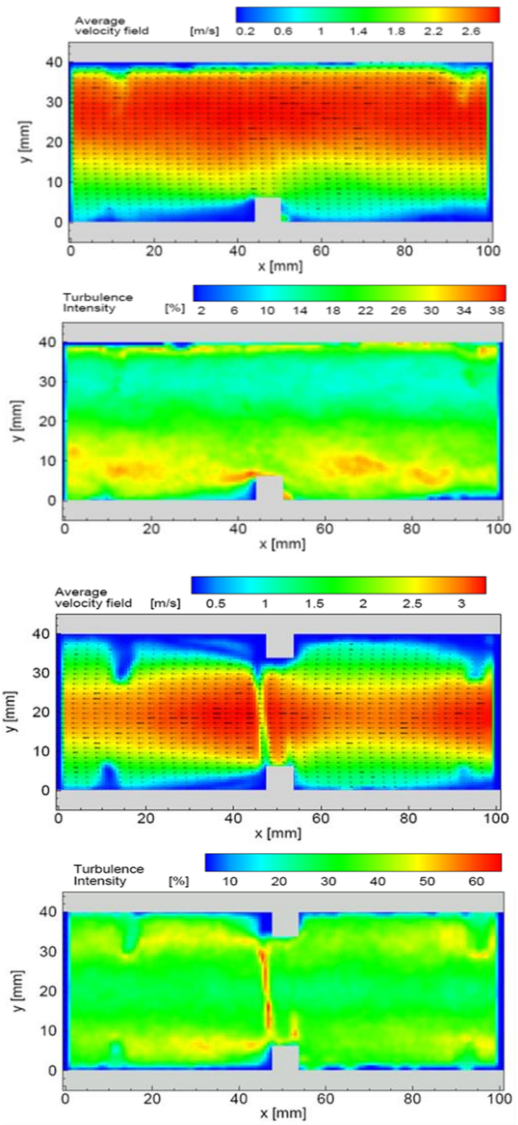

Fig. 20. PIV measurements for ribbed channel and Re = 9000: averaged velocity field and turbulence intensity for geometry with ribbed walls – upper for configuration 13a, and lower for configuration 13b [50].

Figure 20 shows an average velocity field and turbulence intensity (averaged over 100 instantaneous velocity fields) for a geometry with a ribbed bottom wall and ribbed bottom and top wall (ribs height is 6 mm) and flow perpendicular to the ribs (geometry a and b in Fig. 13). The Reynolds number is 9000 and the maximum velocity for these cases is about 3.0 m/s located in the top part of the channel. It also shows that the flow is turbulent with the maximum turbulence intensity about of 38% in the vicinity of the rib and a relatively small turbulence intensity in the top part of the channel (about 10%). In the case presented in Fig. 20, the maximum turbulence intensity is higher than 65% and located in the middle of the channel close to the ribs.

6.3. Natural convection in a closed cavity

The liquid crystal technique was used not only in air flows, but also in other fluids. The distributions of the temperature field and velocity vectors were visualized using a liquid crystal in a pure solution form or microcapsules, either as trace particles inside the fluid or as a coating of the flowing surface. The encapsulated form of the liquid crystal can be mixed directly with water, glycerine or silicone oil. It is recommended to create dilute solutions, i.e. 0.01–0.02% by weight. Too much liquid crystal causes a milky colouration of the diluent, and reflected light causes blurring of colours. The structure of the flow together with the movement of the molecules can be recorded using a camera or a camcorder. Together with the flash of the light knife "cutting through the flow", both the temperature of the molecule (colour) and the direction of the flow (when we take several pictures of one molecule) can be recorded. The undisputed leader in the study of fluid behaviour in closed spaces is T. Kowalewski [27–29,32]. Figure 21 shows the measurement results obtained by him in the cavity (filled with water) under conditions of free convection.

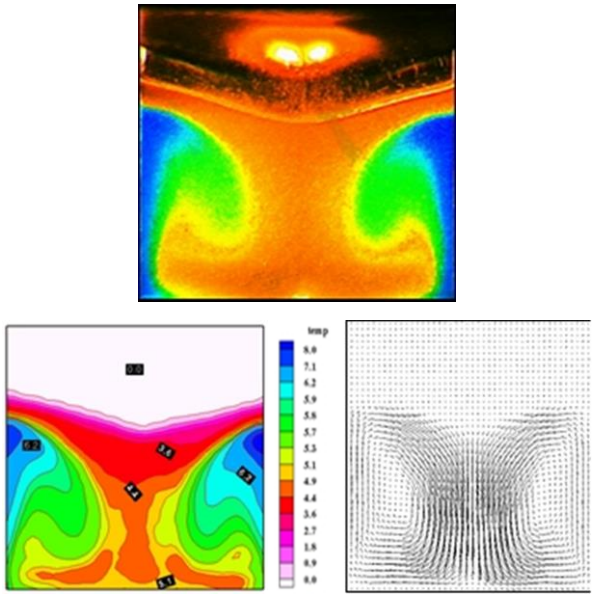

Fig. 21. Freezing of water under a cold surface in a lid cooled cavity. Recorded image of TLC tracers (up), evaluated temperature and velocity fields (down). Time step: 3600 s after cooling starts; isothermal lid temperature $T_c = -10^{\circ}C$, external temperature $T = 20^{\circ}C$ [16,27,28].

In the second experiment (as an example of TLC applications), there was a visualization of free convection in a closed space with glycerol (cavity) with dimensions L = 180 mm of length, H = 30 mm of height and W = 60 mm of width. The white light source in which the moving particles of liquid crystal were observed was a Xenon Flash Lamp. Colour images of moving particles were recorded at intervals of 1 to 15 seconds. Usually, several shots were recorded on one film frame. This colour anemometry resembling PIV was extended with temperature measurement, creating the so-called PIVT (particle image velocimetry and thermometry). Based on the photograph obtained in this way, two-dimensional velocity and temperature fields can be determined. An example of a two-dimensional velocity and temperature field is shown in Fig. 22. The photographs were taken from a horizontal to a vertical position every 30 degrees. Among other things, coloured Benard cells were recorded for the first time.

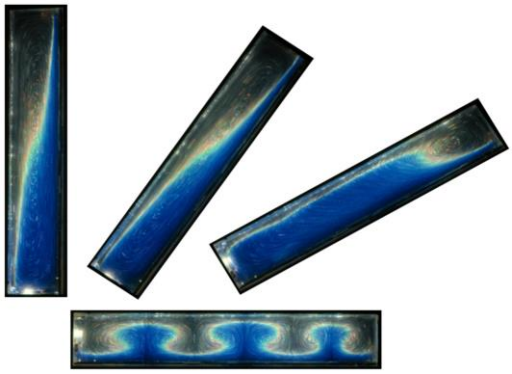

Fig. 22. Temperature and velocity visualisation in glycerol-filled cavity under free convection using TLC ($Ra = 1.2 \cdot 10^4$, $Pr = 12.5 \cdot 10^3$); D_T = 10 K; dimension of cavity: L= 180 mm, H = 30 mm, W = 60 mm. The horizontal position showing the Benard cells.

6.4. Flow visualization of gas model turbine blades cooled by air

Effective methods of gas turbine blades cooling and improving of their effectiveness require the use of modern and unique design solutions. Due to the high temperature of the inlet gas to the first gas turbine rims, there is the constructional and technological problem of designing shafts and blades properly cooled so as to prevent blade erosion (while exceeding the melting point).

The cooling system should provide the lowest mixing intensity and the best thermal barrier for the blade. On the other hand, the coolant mass flow has to be minimized as low as possible, because it influences the compressor and engine overall efficiency. However, the experimental set-up presented in this paper is able to provide complementary data of flow-field around film-cooled turbine blades and heat transfer under turbulent conditions. Examples of modified gas turbine blades are shown in Fig. 23 (up). Within this objective, a new experimental technique, inclusively with LCT has been developed and applied to the study of aerodynamic and aerothermal blade turbine design with the effusive cooling concept. Steady-state and transient methods were used during experiments to capture colour images during LCT experiments.

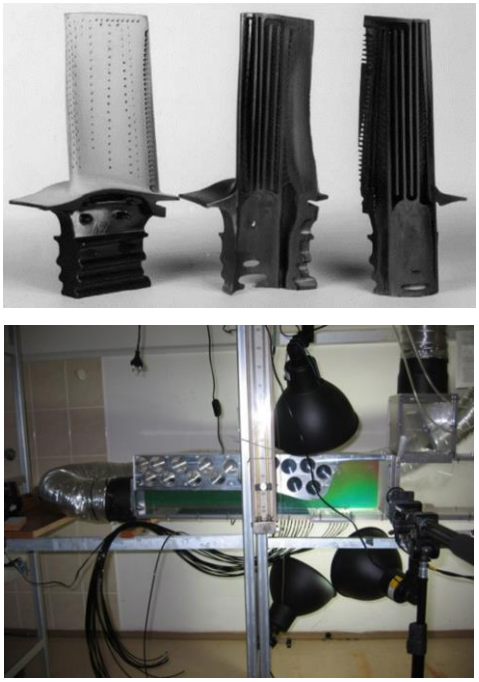

Fig. 23. Gas turbine blades with cooling holes (up) and view of the test section for the model turbine blade cooling system (down) [35].

6.4.1. Experimental facility

Experiments were carried out in a modernized open low-speed wind tunnel presented in Chapter 5 (Fig. 12). The air is pumped into the system through the fan with an automatic speed regulation, which allows us to change the flow over a wide speed range in the further part of the research section. The air flowing out from the checking section goes afterwards to the diffuser section followed by the stabilizing section and subsequently to the test section, which is the last section of the component wind tunnel and is illuminated by the annular lamps, which are commonly used in photography.

The colour temperature of light obtained through these lamps is 5000 K and is similar to daylight. It is also important to have a uniform density of luminous intensity of light in the measuring section so that the four cameras can work and record the experiment in the same range of parameters of light. The brightness of the lamps also affects the optical density parameter of the CMOS sensors of the installed cameras. Four special high speed cameras designed for taking high quality images are used, which allow us to transfer frames at a speed of 87 FPS.

The cameras are equipped with modern Pentax lenses with a focal length of 6 mm that enables us to obtain high quality images from a distance of 20 cm from the object, and two spherical lenses. The lens has a high brightness (f 2.9) and a viewing angle 57°. The white balance of the camera and the shutter are set individually for each camera when changing the location and lighting within the measuring section. The cameras are connected to the computer using the GBit Ethernet cable. The computer has specially designed software, which synchronizes all of the cameras to trigger at the same time. This enables the camera to take four different images of one object made at the same time determined to an accuracy of 2 ms. The software also allows us to store data as a single frame to BMP, and each frame is described in detail and includes a timestamp. Subsequently, frames are stored on a disk storage, where they are collected for further processing by the main computer.

The lower part of the test section is constructed as a flat channel made of plexiglass with a thickness of 8 mm, and the upper side is closed by a modified blade profile made of aluminium. The jet section for secondary flow consists of 16 holes with 2 mm diameter each. The jet section can be located at different positions along the profile. They are marked as 1–2, 3–4, 5–6, 7–8 and 9–10 (Fig. 24).

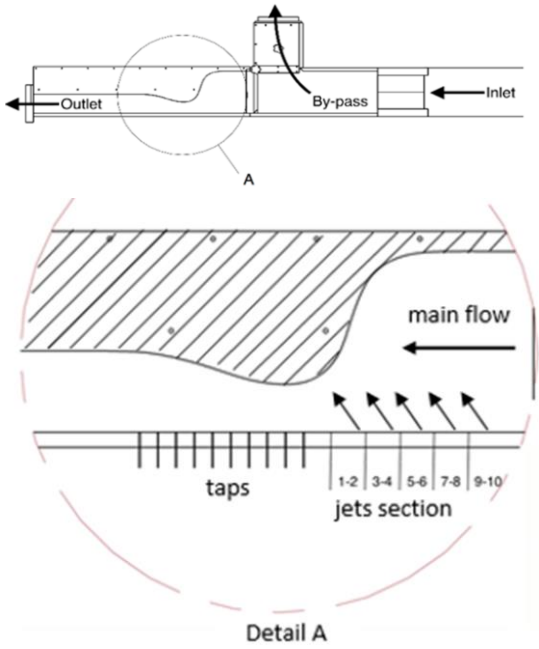

Fig. 24. View section of model turbine blade geometry [34].

For the experimental principle pressure transducers, air flow meters and thermocouples were selected and installed at specific locations in the test rig to measure the pressure, flow rate and temperature for the main and secondary flows. The test section is equipped with a bypass, which enables different air flows for use with transient as well as steady-state LCT techniques (Fig. 24).

Numerical simulations for the section design were carried out in order to obtain the pressure distribution in the channel similar to the blade cascade. The simulations were performed by means of the FINE/Turbo NUMECA code with the Autogrid 5 mesher for cascade configuration.

An example of velocity and static pressure contours in the blade passage is shown in Fig. 25. Numerical simulations for the cascade allow us to determine the pressure distribution on the profile wall, which is considered the reference for the test section design. In Fig. 26 (up), an example of pressure distribution for the test section is shown. It is compared with the results obtained for the cascade. The velocity magnitude distribution at the middle plane of the designed test section is shown in Fig. 26 (down). A properly adjusted shape of the upper wall provides the desired pressure distribution on the lower flat wall. The experimental investigations are carried out on the lower wall.

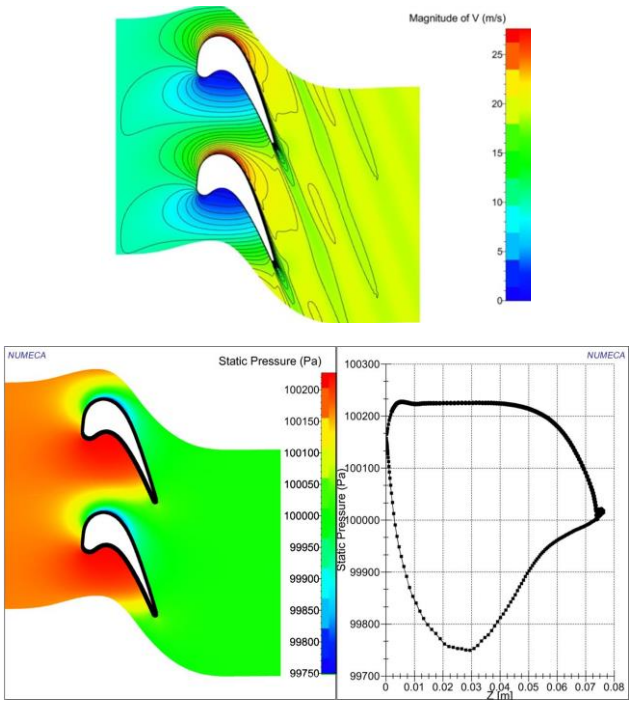

Fig. 25. Velocity magnitude in cascade (up) and static pressure cascade (down) [34].

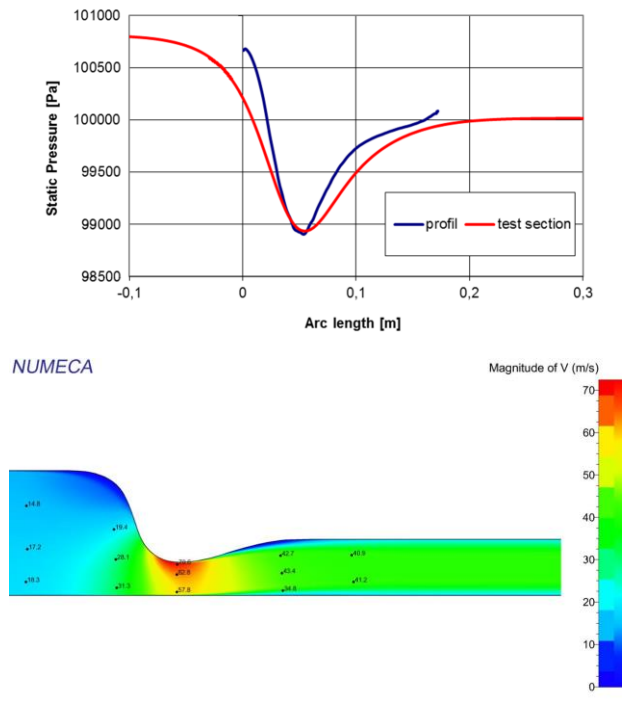

Fig. 26. Static pressure distribution on the suction side of the profile and flat plate (up) and velocity in the test section (down) [34].

6.4.2. Results of LC experiments

The selected results of LCT measurements of steady-state flow are shown below. The experiment was conducted for 3 Reynolds numbers (Re = 87 000, Re=105 000 and Re = 122 000) of air flow in the main channel and for two overpressures (ΔP): ΔP = 5% and ΔP = 15%. The relative pressure or overpressure is defined as a difference between the total pressure at the inlet to the set of jets and that of the main flow inside the channel. Figure 27 presents a visualisation of air flow on the blade surface for Re = 105 000, which corresponds to a velocity of 12 m/s. Figure 28 presents similar results, but for Re = 122 000, which corresponds to a velocity of 14 m/s and for the jet section located at position 7–8. In both examples, hue is converted to the Kelvin temperature using the curve of the calibration nomogram.

Fig. 27. Visualization of air flow on blade surface. Jet position 1–2, Re = 105 000, T_a = 315 K, T_j = 299 K, T_{av} = 313.3 K, ΔP = 5% [51].

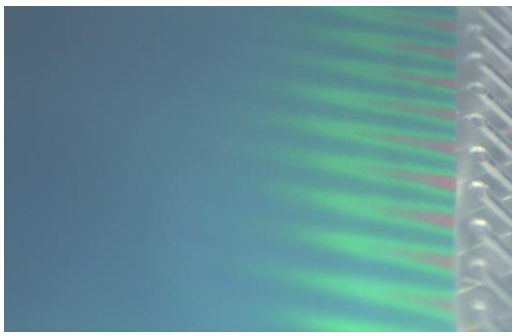

Fig. 28. Visualization of air flow on blade surface. Jet position 7–8, Re = 122 000, T_a = 315 K, T_j = 299 K, T_{av} = 310.9 K, ΔP = 15% [51].

The jet section of the secondary flow is located inside the test section at position 1–2 (see Fig. 24), which is the closest to the profile narrowing. The temperature of air in the main channel was equal T_a = 315 K, while the temperature of air coming from jets was equal T_j = 299 K, and the average temperature of the surface covered by liquid crystal foil T_{av} = 310.9 K; this is an average temperature for the flat plate covered by liquid crystals sheets and "washed" by air. The local hue values versus distance from the jets outlet are presented in Fig. 29.

The results of cooling effectiveness visualization in the turbine inter-blade passage (at the end-wall) using transient LCT measurements are shown in Fig. 30. In this figure, a colour image was obtained with the use of liquid crystals thermography for Re = 122 000 and transient performance.

Measurements were taken for a few time steps, calculated from the moment of hot air entry to the test section (t+ is time in seconds). Before the measurements, hot air flowed through a bypass and then was directed to the test section by a three-way

valve. The air temperature was kept constant and equal T_a = 315 K. Recently the steady-state technique of LCT has been used by F. Satta and G. Tanda [33] to map the heat transfer coefficient distributions at the end-wall of the turbine blade cascade.

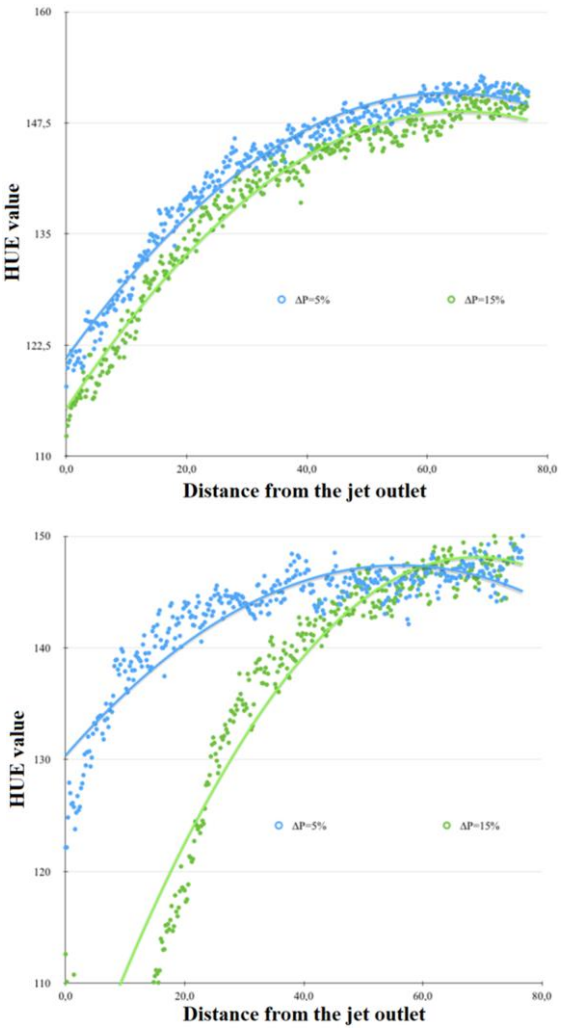

Fig. 29. Local hue value versus distance from jets outlet. Jets position 1–2, Re = 105 000, T_a = 315 K, T_j =299 K (up), jets position 7–8, Re = 122 000, T_a = 315 K, T_j =299 K (down) [51].

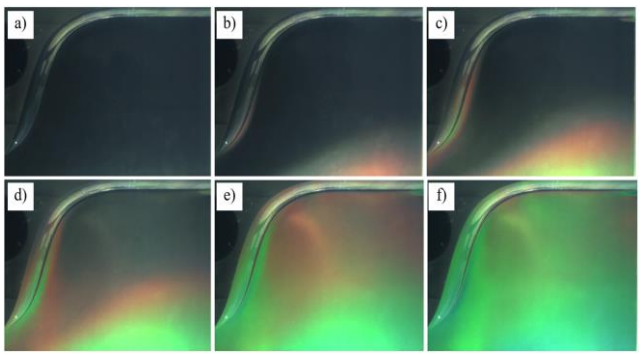

Fig. 30. End-wall of model turbine blade temperature distribution: colour image. Re = 122000, T_a = 315 K, t+12s, time steps: a) t+0s, b) t+4s, c) t+8s, d) t+12s, e) t+16 s, f) t+20s [50].

6.5. Investigations of using TLC in defectoscopy

Strugała et al. [51] proposed and described a new method for non-invasive testing of impact damage in carbon fibre reinforced polymer (CFRP) using thermo-optical techniques (Fig. 31). Compared to previously used techniques, for example computer radiography (CR), this method is low-cost and does not require complicated equipment. Since the recording takes place using conventional cameras (see Fig. 32), this method can also be used in field research. The comparative analysis showed that this technique can be a full-fledged accurate tool for an NDT method for the diagnosis of impact damage in CFRP (Fig. 33).

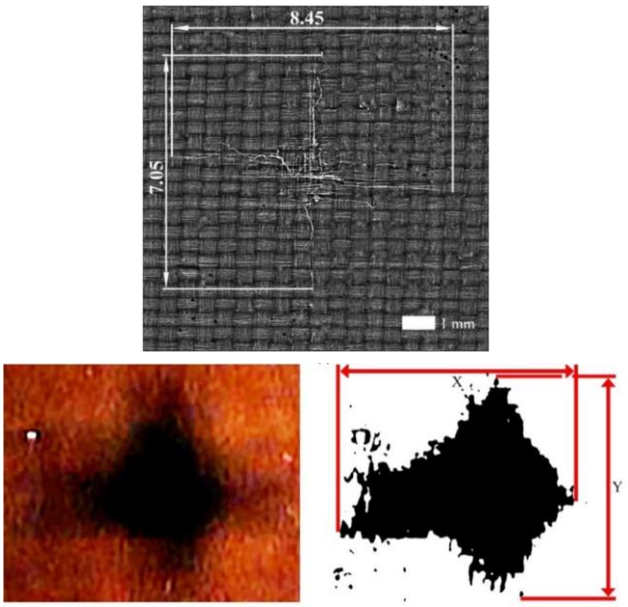

Fig. 31. X-ray image of cracked CFRP sample (up), TLC image of damaged area and its post-processing for quantitative analysis (down).

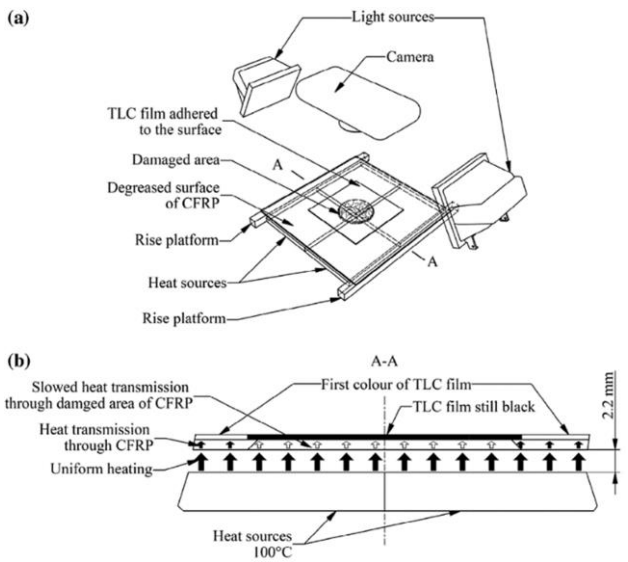

Fig. 32. Schematic drawings of (a) experiment station for sheet of laminated thermochromic liquid crystal film tests, (b) cross-section (A–A) with representation of heat transmission through an impacted specimen with the adhered sheet of laminated TLC film.

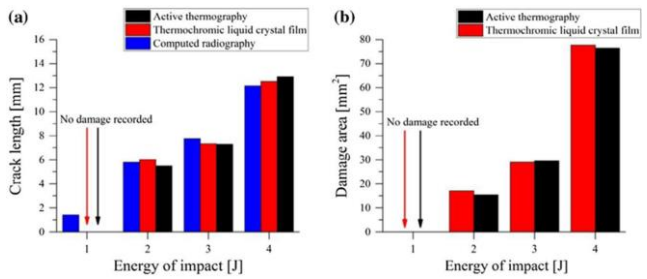

Fig. 33. Comparison of the NDT methods depending on the impact energy where: (a) comparison of the average crack length vs impact energy for three NDT methods, (b) comparison of the damage area vs impact energy measured by means of active thermography and laminated thermochromic liquid crystal film.

The use of liquid crystals significantly reduces the hardware costs of diagnostics without affecting the quality of results, compared to expensive thermal imaging cameras. The key disadvantages of the TLC film technique are negligible in terms of the applied procedure for performing the tests.

6.6. Medical applications

In medical applications, thermochromic liquid crystal and infrared thermography are used for examinations of breast cancer, thyroid dysfunction, lymphatic congestion, vascular and nervous system disorders, abdominal inflammation, muscle disorders, rheumatological conditions, orthopaedic diseases and many others [37–42]. It is used for both men and women. Diagnostics and prevention are definitely a better and cheaper solution than treatment. This is also the purpose of medical thermography, a test that allows you to visualize physiological changes in the body in the early stages of their development.

Thermography is a state-of-the-art non-invasive screening procedure (non-contact, radiation-free) that uses heat detection to locate areas of temperature differences in the body. Most pathological processes manifest themselves as increased heat, and some neurological processes exhibit excessive cold or hypothermia. For example, breast disease can be detected by looking for areas of excessive or increasing heat, which may indicate areas of angiogenesis or growth of blood vessels supplied by a growing tumour.

Unlike X-ray, ultrasound magnetic resonance imaging (MRI), and virtually all other modern medical imaging modalities are designed to capture anatomical information, while thermochromic liquid crystal and medical infrared technology are designed to capture more physiological information. Examples of two thermograms of human hands performed by LCT (left) and DII (right) [42,50] are shown in Fig. 34.

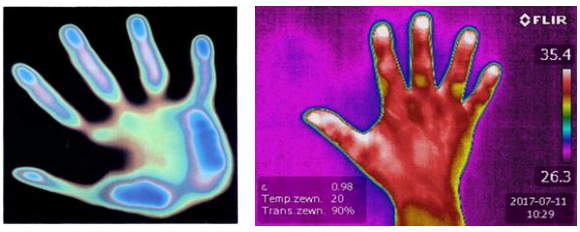

Fig. 34. Examples of two thermograms of human hands performed by LCT (left) and DII (right) [42,50].

6.6.1. Breast thermography

The distribution of temperature on the surface of the human body is determined by the temperature of the tissues of internal organs, the thermal conductivity of muscle and fat tissue, and the thermal emission of the skin. Hence, the temperature measured on the skin surface is a function of temperature of the internal organ and thermal properties of the tissues separating this organ from the body surface. An important role is also played by the processes of heat losses by convection and radiation through the skin, including gas exchange between the skin and the environment. Thermographic examinations are used both in the assessment of changes recorded on the skin surface and in relation to parenchymal organs located close to the skin surface. They provide opportunities for monitoring the circulatory system in both large and small vessels. It should be emphasized that very often temperature changes are one of the earliest symptoms of ongoing pathological processes. Therefore, both diagnostic methods, i.e. LCT and DII, are suitable for breast cancer screening (see Figs. 35 and 36).

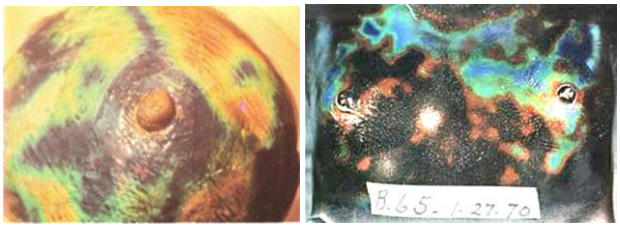

Fig. 35. Two examples of detection of breast cancer (dark region) by liquid crystal thermography. The blue and dark colours correspond to the higher temperature caused by inflammation [39].

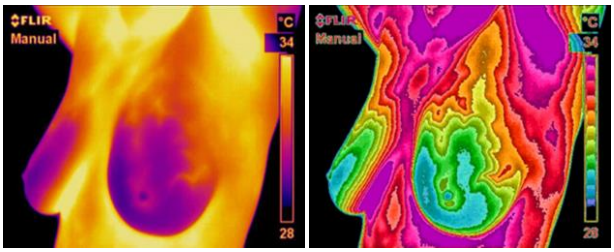

Fig. 36. Infrared image of human breast – left and a normal limited vascular pattern – right [38].

This kind of medical diagnosis (Figs. 35 and 36) should be confirmed by other independent methods (mammography ultrasound and MRI) in the case of disease suspicions.

6.6.2. Orthopedic application of LCT

In clinical studies of unspecified inflammatory conditions of orthopaedic diseases, liquid crystal thermography (LCT) can help in their identification. With its help, it is possible to localize the change and its extent, which may have an inflammatory, post-traumatic, degenerative, infectious or neoplastic origin. Most of these cause changes in the temperature of the synovial membrane and connective tissue, which can be recorded using very sensitive liquid crystals. On the basis of such changes, the level

of pathological changes can be estimated very quickly, and an example of such a disease is Raynaud's and Buerger's phenomenon, the pathological changes of which are presented using a thermogram as shown in the figures bellow:

- Raynaud's phenomenon (Symptoma Raynaud) is a vasomotor disorder characterized by sudden, well-demarcated blanching, then cyanosis and redness of the fingers, toes and rarely the nose and auricles, accompanied by numbness and pain. This happens because of spasms of blood vessels in those areas. The spasms happen in response to cold, stress or emotional upset (Fig. 37).

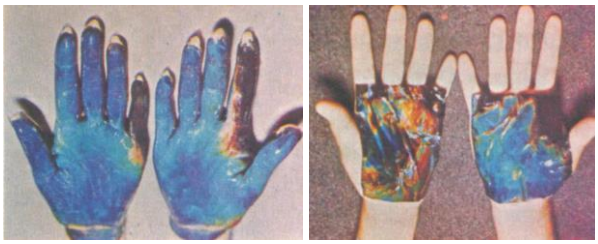

Fig. 37. Raynaud LC thermograms of vascular disease (left), and hand tumours (right) [40].

- Buerger's disease (known as Thromboangiitis Obliterans), is an inflammation of small and medium-sized blood vessels. Although any blood vessel can be affected, it usually presents with blockages in the arteries in the feet and hands, leading to severe pain and tissue damage (Fig. 38).

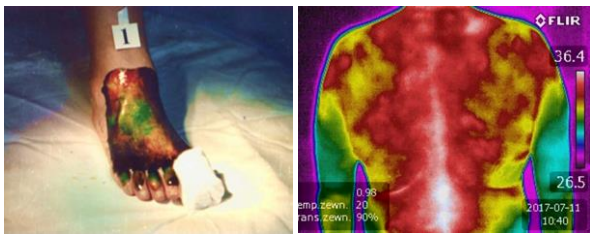

Fig. 38. Visualisation (by use of LCT) of lack of blood circulation caused by Buerger's disease (left) and DII thermogram of human back effected by muscular tensions (right) [39,50].

6.7. Advantages and disadvantages of TLC and DII

For surface or human body temperature measurement, special care is necessary to avoid specula light reflections form, irradiating or pulses, however some advantages and disadvantages of the use of TLC and DII are presented below:

❖ Advantages of TLC:
- Provides a quick visual qualitative observation of the surface temperature profile.
- Can be calibrated with a digital colour camera and isothermal surface control to provide accurate quantitative temperature fields to +/− 0.1°C.
- Typically operate between –30°C to 120°C with bandwidths of 0.1°C to 30°C.
- A high spatial resolution of around 1 μm, depends on camera optics.
- Provides both transient and steady-state surface temperature profiles.
- A fast time response of around 100 ms.
- Thermometry uses visible light and is independent of surface emissivity.
- Relatively cheap technique: camera, recorder, lighting etc.

❖ Disadvantages of TLC:
- Requires a stable uniform white light source with no infrared IR or ultraviolet UV components.
- IR will cause radiant heating of the surface, and UV will degrade the liquid crystal compounds.
- Must be calibrated in-situ using the same optics as the final experiment.
- Test subject must be prepared before measurements and the liquid crystals can be difficult to apply to complex surface geometries.
- Can be intrusive due to changes in the heat conduction properties of the body.
- Cannot be used for large subjects such as houses etc.

❖ Advantages and disadvantages of DII.
- Thermography has been shown effective as a standalone test for either breast cancer screening or diagnosis in detecting early stage breast cancer.
- Thermography has only been cleared by the official regulatory as an “adjunctive “ tool – meaning for use alongside a primary test like mammography.
- Thermogram is no substitute for mammogram, it works by detecting increases in temperature.
- If the thermography detects any abnormalities, the person should seek further screening, which may include a mammogram. If a mammogram confirms that a lamp is present, the doctor may recommend an ultrasound or MRI scanning and a biopsy.
- Thermography produces a high number of false-positive and false-negative results and estimates of its sensitivity vary widely.
- In a positive way, thermography offers the following benefits: it is not painful, it is not invasive and it does not involve radiation.

7. Conclusions

Advanced experimental techniques, in this case, true-colour image processing of liquid crystal patterns, particle image velocimetry and infrared imaging allow new approaches to old problems and open up new areas of research and applications. Image processing data make available quantitative full field information about the distribution of temperature, heat transfer and adjunctive medical pathogenesis and diagnostics. It is evident from our research that liquid crystal and infrared imaging techniques have many applications, not only in testing but also in industry, medicine and home.

The presented overview provides an introduction to thermochromic liquid crystals, digital infrared imaging and particle image velocimetry, how these measurement techniques and methods work and how they are used.

References

[1] Baughn, J.W., Ireland, P.T., Jones. T.V., & Saniel, N. (1989). A comparison of the transient and heated-coating methods for the measurement of local heat transfer coefficients on a pin fin. *ASME Journal of Heat and Mass Transfer*, 111(4), 871−881. doi: 10.1115/1.3250800

[2] Bergles, A.E. (1997). Augmentation of heat transfer, single phase. In: *International encyclopaedia of heat and mass transfer* (Ed. Hewitt G.F., Shires G.L., Polezhaev Y.V.), 68−73, CRC Press, Boca Raton, Florida, USA.

[3] Ciofalo, M., Di Piazza I., & Stasiek, J.A. (2000). Investigation of flow and heat transfer in corrugated-undulated plate heat exchangers. *Heat and Mass Transfer*, 36, 449−462. doi: 10.1007/S002310000106

[4] Fiebig, M. (1996). Vortices: tools to influence heat transfer – recent developments. *Proceeding of 2nd European Thermal-Sciences and 14th UIT National Heat Transfer Conference*, 1, (pp. 41−56), 29−31 May, Rome. Italy.

[5] Fiebig, M., & Mitra, N.K. (1998). Experimental and numerical investigation of heat transfer enhancement with wing-type vortex generators. Chapter 8. In: *Computer Simulations in Compact Heat Exchangers*, (Ed. Sunden B., Faghri M.), *Computational Mechanics Publications*, 1, (pp. 227−254), Southampton, UK and Boston, USA

[6] Hippensteele, S.A., Russel, L.M., & Stepka, F.S. (1983). Evaluation of a Method for Heat Transfer Measurements and Thermal Visualization Using a Composite of a Heater Element and Liquid Crystals. *International Journal of Heat and Mass Transfer*, 105(1), 184−189. doi: 10.1115/1.3245539

[7] Jacobi, A.M., & Shah, R.K. (1995). Heat Transfer Surface Enhancement Through the Use of Longitudinal Vortices: A Review of Recent Progress. *Experimental Thermal and Fluid Science*, 11(3) 295−309. doi: 10.1016/0894-1777(95)00066-U

[8] Jones, T.V., & Hippensteele, S.A. (1998). *High-resolution heat transfer coefficient mops applicable to compound-curve surfaces using liquid crystals in a transient wind tunnel*. NASA Technical Memorandum 89855.

[9] Jones, T.V., Wang, Z., & Ireland, P.T. (1992). The use of liquid crystals in aerodynamic and heat transfer experiments. *Proc. 1st I. Mech. E. Seminar on optical methods and Data Process-ing in Heat and Fluid Flow*, 51−54, City University, London, UK.

[10] Leiner, W., Schulz, K., Behle, M., & Lorenz, S. (1996). Imaging techniques to measure local heat and mass transfer. *Proc. 3nd I. Mech. E. Seminar Optical Methods and Data Processing in Heat and Fluid Flow*, 1−13, City University, London, UK.

[11] Mikielewicz, D., Stasiek, A., Jewartowski, M., & Stasiek, J. (2012). Measurements of heat transfer enhanced by the use of transverse vortex generators. *Applied Thermal Engineering*, 49, 61−72. doi: 10.1016/j.applthermaleng.2011.11.013

[12] Simonich, J.C., & Moffatt, R.J. (1982), New technique for mapping heat transfer coefficient contours. *Review of Scientific Instruments*, 53(5), 678−683. doi: 10.1063/1.1137041

[13] Stasiek, J. (1998). Experimental study of heat transfer and fluid flow across corrugated-undulated heat exchanger surfaces. *International Journal of Heat and Mass Transfer*, 41, 899−914. doi: 10.1016/S0017-9310(97)00168-3

[14] Stasiek, J. (1997). Thermochromic liquid crystals and true-colour image processing in heat transfer and fluid flow research. *Heat and Mass Transfer*, 33, 27−33, Springer-Verlag. doi: 10.1007/S002310050158

[15] Stasiek, J., Ciofalo, M., & Wierzbowski, M. (2004). Experimental and Numerical Simulations of Flow and Heat Transfer in Heat Exchanger Elements Using Liquid Crystal Thermography. *Journal of Thermal Science*, 12(2), 133−137. Article ID: 1003-2169(2004)02-0133-05

[16] Stasiek, J.A., & Kowalewski, T.A. (2002). Thermochromic liquid crystals applied for heat transfer research. *Opto-Electronics Review*, 10(1), 1−10.

[17] Stasiek, J., Stasiek, A., Jewartowski, M., & Collins, M.W. (2006). Liquid crystal thermography and true-colour digital image processing. *Optics & Laser Technology*, 38(4−6,), 234−256. doi: 10.1016/j.optlastec.2005.06.028

[18] Tanda, G. (2001). Heat Transfer and Pressure Drop in a Rectangular Channel With Diamond-Shaped Elements. *International Journal of Heat and Mass Transfer*, 44, 3529–3541. doi: 10.1016/S0017-9310(01)00018-7

[19] Tanda, G. (2004). Heat Transfer in Rectangular Channels With Transverse and V-Shaped Broken Ribs. *International Journal of Heat and Mass Transfer*, 47, 229–243. doi: 10.1016/S0017-9310(03)00414-9

[20] Tanda, G., & Abram, R. (2009). Forced Convection Heat Transfer in Channels With Rib Turbulators Inclined at 45 deg. *ASME Journal of Turbomachinery*, 131. doi: 10.1115/1.2987241

[21] Tanda, G., Stasiek, J., & Collins, M.W. (1995). Application of holographic interferometry and liquid crystal thermography to forced convection heat transfer from a rib-roughened channel. *8th Int. Conference on Energy and Environment* (pp. 434−441), Shanghai, China. doi: 10.1615/1-56700-052-5.610

[22] Utriainen, E., & Sunden, B. (2002). Evaluation of the Cross Corrugated and Some Other Candidate Heat Transfer Surfaces for Microturbine Recuperators. *ASME Journal of Engineering for Gas Turbines and Power*, 124 (3). doi: 10.1115/1.1456093

[23] Valencia, A., Fiebig, M., Mitra, N.K., & Leiner, W. (1992). Heat transfer and flow loss in a fin-tube heat exchanger element with wing-type vortex generators. *Heat Transfer, 3rd UK National Conference Incorporating 1st European Conference on Thermal Sciences*, 16−18 September, Birmingham, UK.

[24] Vogel, G., Graf, A.B.A., von Walfersdorf, J., & Weigand, B. (2003). A Novel Transient Heater-Foil Technique for Liquid Crystal Experiments on Film-Cooled Surfaces. *ASME Journal of Turbomachinery*, 125, 529−537. doi: 10.1115/1.1578501

[25] Wierzbowski, M., & Stasiek, J. (2002). Liquid crystals technique application for heat transfer investigation in a fin-tube heat exchanger element. *Experimental Thermal and Fluid Science*, 26, 319−323. doi: 10.1016/S0894-1777(02)00143-7

[26] Hiller, W.J., & Kowalewski, T.A.(1986). Simultaneous measurements of temperature and velocity fields in thermal convective flows. In: *Flow Visualization IV* (Ed. Veret C., pp. 617−622). Hemisphere Publishing Corporation. Washington.

[27] Kowalewski, T.A., & Cybulski, A. (1996). Experimental and numerical investigations of natural convection in freezing water. *Int. Conference on Heat Transfer with Change of Phase in Mechanics*, Mechanics, 61, 7−16, Kielce, Poland.

[28] Kowalewski, T.A., Cybulski, A., & Rebow, M.(1998). Particle image velocimetry and thermometry in freezing water. *8th International Symposium On Flow Visualization*, Sorrento (Ed. Carlomagno G.M. and Grant I.), CD ROM Proc., 24.1−24.8, Edinburgh.

[29] Kowalewski, T.A., & Rebow, M.(1999). Freezing of water in the differentially heated cubic cavity, *International Journal of Computational Fluid Dynamics*, 11(3), 193−210. doi: 10.1080/10618569908940874

[30] Raffel, M., Willert, Ch.E., & Kompenhans, J. (1998). *Particle Image Velocimetry* (1st ed.). Springer Berlin, Heidelberg, Germany. doi: 10.1007/978-3-662-03637-2

[31] Tanaka, T. (1998). Visualisation of the temperature field in thermal storage tanks by using the thermosensitive liquid crystals sus-

pension method. *International Symposium Fluid Control, Measurement, Mechanics and Flow Visualisation*, 212−215.
[32] Tropea, C., Yarin, A.L., & Foss, J. (Eds). (2007). *Springer Handbook of Experimental Fluid Mechanics*. Springer-Verlag, Berlin, Heidelberg. Germany.
[33] Satta, F, & Tanda, G. (2014). Measurement of local heat transfer coefficient on the end wall of a turbine blade cascade by liquid crystal thermography. *Experimental Thermal and Fluid Science*, 58, 209−215. doi: 101016/j.expthermflusci.2014.07.005
[34] Borda, T., Flaszyński, P., Doerffer, P., Jewartowski, M., & Stasiek, J. (2015). Flow visualization and heat transfer investigations on the flat plate with stream-wise pressure gradient. *12th International Symposium on Experimental Computational Aerothermodynamics of Internal Flows*, Lerici, Italy.
[35] Ekkad, S.V., & Singh, P. (2021). Liquid Crystal Thermography in Gas Turbine Heat Transfer. A Review on Measurement Techniques and Recent Investigations. *Crystals*, 11(11) 1332, doi: 10.3390/cryst11111332
[36] Reinitzer, R. (1888). Beiträge zur Kenntniss des Cholestrins. *Monatshefte für Chemie*, Wien, 9, 421−441. doi: 10.1007/ BF01516710
[37] Polidori, G., Renard, Y., Lorimier, S., Pron, H., Derrau, S., & Taiar, R. (2017). Medical Infrared Thermography assistance in the surgical treatment of axillary Hidradenitis Suppurativa: A case report. *International Journal of Surgery Case Reports*, 34, 56−59. doi: 10.1016/j.ijscr.2017.03.015
[38] Seymour, T. (2019). *Breast thermography: what you need to know*. https://www.medicalnewstoday.com [accessed 22 Jan. 2025].
[39] Żmija, J., Klosowicz, S., & Borys, S. (1989). *Cholesteric Liquid Crystals in a Detection of Radiation*. WNT, Warsaw (in Polish).
[40] Shlens, M., Stoltz, M.R., & Benjamin, A. (1975). Orthopaedic applications of liquid crystal thermography. *The Western Journal of Medicine*, 122, 367−370.
[41] Podbielska, H., & Skrzek, A. (Eds.). (2014). *Biomedical applications of thermovision*. Wroclaw University of Technology, Poland (in Polish).
[42] Stasiek, J., & Jewartowski, M. (2017). Liquid Crystals, PIV and IR-Photography in Selected Technical and Biomedical Applications. *IOP Conf. Series: Materials Science and Engineering*, 249, 012010. doi: 10.1088/1757-899X/249/1/012010
[43] Kesztyüs, D., Brucher, S., Wilson, C., & Kesztyüs, T. (2023). Use of Infrared Thermography in Medical Diagnosis, Screening, and Disease Monitoring, A Scoping Review. *Medicina*, 59(12), doi: 10.3390/medicina59122139
[44] Moffat, R. J. (1990). Experimental Heat Transfer. *Proc. 9th Int. Heat Transfer Conference*, 1, 187–205, 19−24 August, Jerusalem, Israel. doi: 10.1615/IHTC9.1900
[45] Dierking, I. (2014). Chiral Liquid Crystals: Structures, Phases, Effects. *Symmetry*, 6(2), 444−472. doi: 10.3390/sym6020444
[46] Klein, E.J. (1968). Application of liquid crystals to a boundary layer flow visualisation. *American Institute of Aeronautics and Astronautics. Meeting: Aerodynamic Testing Conference*, 8−10 April, San Francisco, USA.
[47] Klein, E.J., & Margozzi, A.P. (1969). *Exploratory investigation on the measurement of skin friction by means of liquid crystals*. NASA TM-X-1774.
[48] Stasiek, J., & Collins, M.W. (1996). The use of liquid crystals and true-colour image processing in heat and fluid flow experiments. *Atlas of Visualization*, 2, CRC Press, Inc., New York, USA.
[49] Bagavathiappan, S, Lahiri, B.B., Saravanan, T., Philip, J., & Jayakumar, T. (2013). Infrared thermography for condition monitoring – A review. *Infrared Physics & Technology*, 60, 35−55, doi:10.1016/j.infrared.2013.03.006
[50] Stąsiek, J., Jewartowski, M., & Stąsiek, A. (2016). *Liquid crystal thermography and image anemometry in selected technical applications*. AGNI Publisher Pruszcz Gdanski, Poland (in Polish).
[51] Strugała, G., Klugmann, M., Landowski, M., Szkodo, M., & Mikielewicz, D. (2018). A universal NDT method for examination of low energy impact damage in CFRP with the use of TLC film. *Non-destructive Testing and Evaluation*, 33(3), 315−328, doi: 10.1080/10589759.2018.1428323
[52] Bizzarri, M., Conti, P., Glicksman, L.R., Schito, E., & Testi, D. (2024). Evaluation by Liquid Crystal; Thermography of Transient Surface Temperature Distribution in Radiant Floor Cooling Applications and Assessment of Analytical and Numerical Models. *Journal of Heat and Mass Transfer*, 146(5), doi: 101115/1. 4064707
[53] Kumar, D., Choudhury, R., & Layek, A. (2022). Application of liquid crystal thermography for temperature measurement of the absorber plate of solar air heater. *Materials Today; Proceedings*, 59, 605−611, doi: 1016/j.matpr.2021.12.09
[54] Hallcrest Ltd. (2014). *Handbook of Thermochromic Liquid Crystal Technology*. LCR Hallcrest.
[55] C.I.E. (1976). *UCS Chromaticity Diagram*. https://www.ledtronics.com (Google Scholar) [accessed 22 Jan. 2025].
[56] Data Translation Ltd. (1991). *Image Processing Handbook*. USA.
[57] MERC Ltd. (1994). *Poole, Dorset, UK Thermochromic Liquid Crystals – Manufacturer's catalogue*.
[58] B.D.H. Limited. *Advanced Materials Division*. UK.
[59] B & H Liquid Crystal Devices Ltd. (1992). London, UK.
[60] *Beginnings of Quantum Mechanics*. http://260h.pbworks.com [accessed 22 Jan. 2025].

Appendix

Figures 39, 40 and 41 show early results from liquid crystal thermography, where the heat transfer coefficients were determined from colour photographs taken with a photo camera. The resulting temperature distributions and subsequently Nusselt numbers on the surfaces in question were taken manually from the images projected onto a screen and reproduced with hand-coloured markers. For comprehensive quantitative local heat transfer data, the visibly sharp line of the spectrum was obtained at different fluid temperatures for the same Reynolds number. Afterwards as shown above the subsequent thermographic studies were carried out using full automatic colour image processing from Data Translation Ltd., USA.

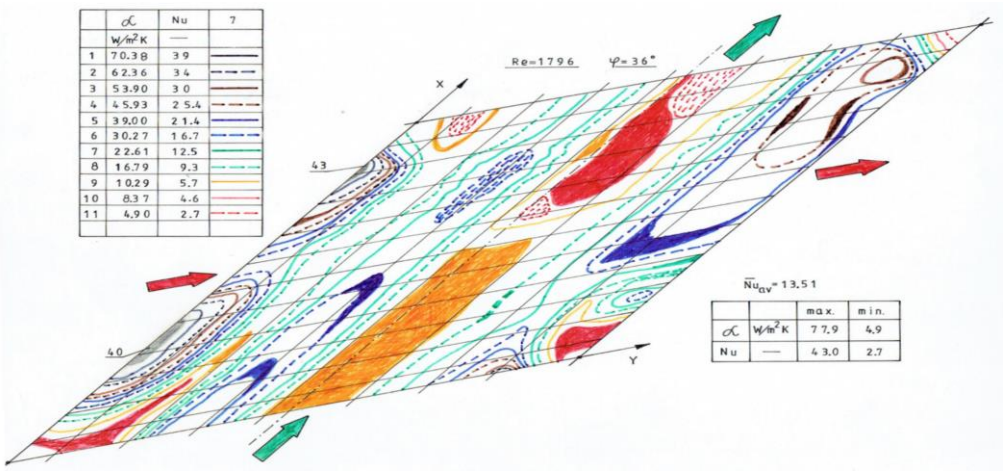

Fig. 39. Visualisation of the distribution of local Nusselt number values on the lower corrugated surface; b = 36 deg, Re = 1796, P/Hi = 3.67 (manual method).

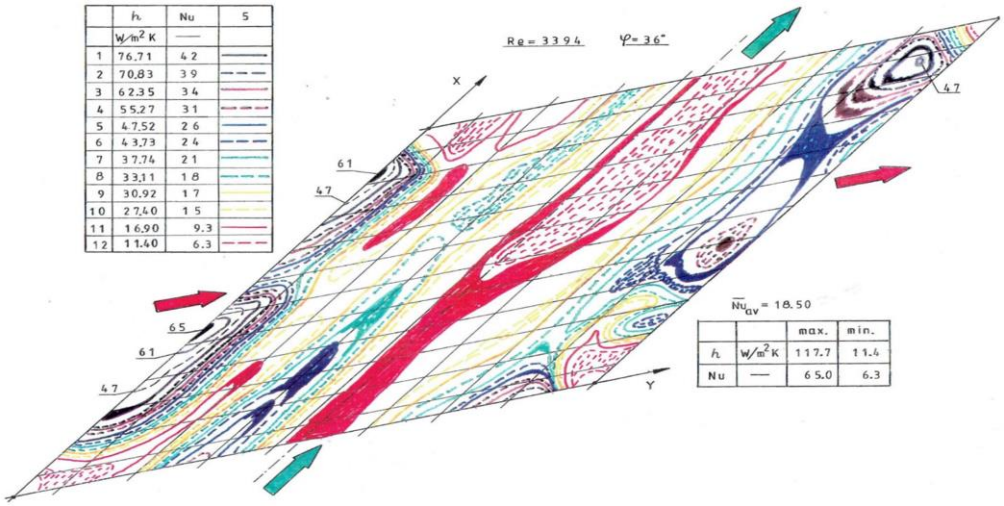

Fig. 40. Visualisation of the distribution of local Nusselt number values on the lower corrugated surface; b = 36 deg, Re = 3394, P/Hi = 3.67 (manual method).

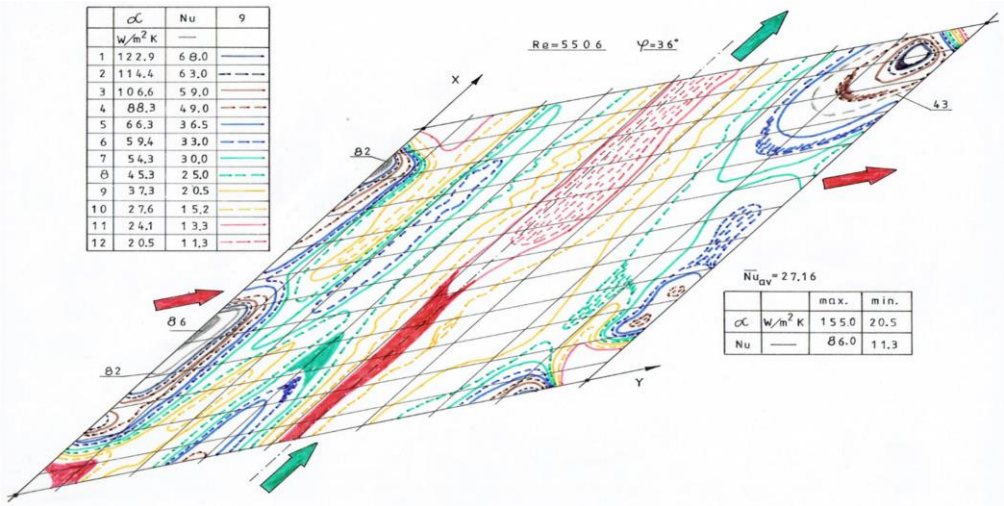

Fig. 41. Visualisation of the distribution of local Nusselt number values on the lower corrugated surface; b = 36 deg, Re = 5506, P/Hi = 3.67 (manual method).